Published in final edited form as:

Biochemistry. 2019 June 18; 58(24): 2730–2739. doi:10.1021/acs.biochem.9b00096.

Non-Additive Effects of Binding Site Mutations in Calmodulin

Sean C. Edington[†,§], **D. Brent Halling**[‡], **Suzanna M. Bennett**[‡,‖], **Thomas R. Middendorf**[‡], **Richard W. Aldrich**[‡], **Carlos R. Baiz**[*,†]

[†]Department of Chemistry, The University of Texas at Austin, Austin, Texas 78712, United States

[‡]Department of Neuroscience, The University of Texas at Austin, Austin, Texas 78712, United States

Abstract

Despite decades of research on ion-sensing proteins, gaps persist in the understanding of ion binding affinity and selectivity even in well-studied proteins such as calmodulin. Site-directed mutagenesis is a powerful and popular tool for addressing outstanding questions about biological ion binding and is employed to selectively deactivate binding sites and insert chromophores at advantageous positions within ion binding structures. However, even apparently nonperturbative mutations can distort the binding dynamics they are employed to measure. We use Fourier transform infrared (FTIR) and ultrafast two-dimensional infrared (2D IR) spectroscopy of the carboxylate asymmetric stretching mode in calmodulin as a mutation- and label-independent probe of the conformational perturbations induced in calmodulin's binding sites by two classes of mutation, tryptophan insertion and carboxylate side-chain deletion, commonly used to study ion binding in proteins. Our results show that these mutations not only affect ion binding but also induce changes in calmodulin’s conformational landscape along coordinates not probed by vibrational spectroscopy, remaining invisible without additional perturbation of binding site structure. Comparison of FTIR line shapes with 2D IR diagonal slices provides a clear example of how nonlinear spectroscopy produces well-resolved line shapes, refining otherwise featureless spectral envelopes into more informative vibrational spectra of proteins.

Graphical Abstract

[*]**Corresponding Author**: cbaiz@cm.utexas.edu.
[§]S.C.E.: Department of Chemistry, Yale University, New Haven, CT 06520.
[‖]S.M.B.: Department of Molecular and Cellular Physiology, Stanford University School of Medicine, Stanford, CA 94305.

Supporting Information

The Supporting Information is available free of charge on the ACS Publications website at DOI: 10.1021/acs.biochem.9b00096.

Supplemental Data, complete FTIR data set (Figure S1), second-derivative spectra for the FTIR data set (Figure S2), and complete 2D IR diagonal slice data set (Figure S3) (PDF)

Accession Codes

NCBI Reference Sequence mRNA: *Rattus norvegicus* calmodulin 2 (Calm2), NM_017326.3. NCBI Reference Sequence protein: *R. norvegicus* calmodulin 2 (CaM2), NP_059022.

The authors declare no competing financial interest.

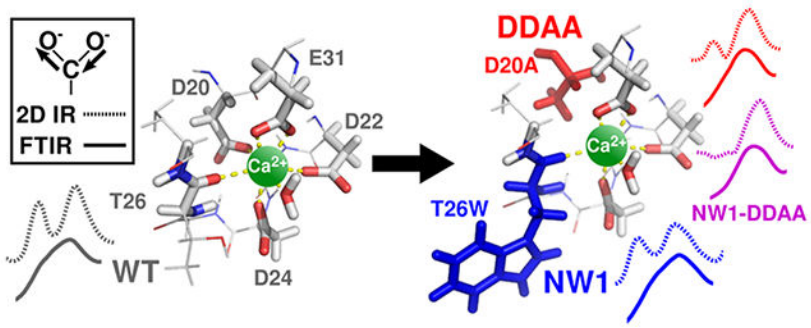

Structural and functional descriptions of the important process of ion binding to proteins remain incomplete.[1–4] This difficulty is partly due to the fact that clear observables marking site-dependent occupancy and ion-dependent conformational changes are often unavailable or difficult to interpret. Site-specific mutagenesis provides the tools needed to engineer useful observables into ion binding proteins, thus facilitating the characterization of binding processes.

However, mutations can perturb the conformation and/or dynamics of proteins, sometimes in subtle ways. For example, mutating a site might not perturb global binding constants but could have local and dynamic effects that are overlooked by measurements sensitive primarily to equilibrium properties.[5] Our previous work showed that even substitution of ions of similar cations for Ca^{2+}, a structural perturbation arguably much less disruptive than mutagenesis, alters the binding site conformation in full-length wild-type (WT) calmodulin[6] and in simple chemical models of ion binding sites such as EDTA.[7] Thus, site-specific mutagenesis may alter the very binding site structures that are being studied despite appearing non-perturbative to functional assays.[8,9]

The calcium binding protein calmodulin (CaM) is ubiquitous in eukaryotes and is the major transducer of eukaryotic Ca^{2+} signals. CaM has two stable, globular lobes[10,11] that each contain a pair of EF-hand Ca^{2+} binding structures. The sequences of CaM's four EF-hands are distinct, yet each is highly conserved.[12]

Here, we investigate two classes of mutations (Figure 1) in N-terminal domain calmodulin (N-CaM). The first class of mutation (termed "NW1") replaces the threonine at position 26 with tryptophan, with the purpose of installing a spectroscopic probe without perturbing ion binding.[5,13] Tryptophan insertions at canonical position 7 in EF-hand sites have been used to detect ion binding in two ways. (i) Their fluorescence is sensitive to conformational changes resulting from ion binding,[5] and (ii) they can sensitize the luminescence of locally bound Tb^{3+}. [14] The second class of mutation (termed "DDAA") replaces ion-coordinating aspartate residues with alanine at canonical position 1 of EF-hands I and II (D20A and D56A mutated at the same time) and is meant to knock out Ca^{2+} binding[15–22] at those sites. Although mutations that disrupt Ca^{2+} binding are often used as tools to mimic the "apo" state of CaM (i.e., CaM in the Ca^{2+}-free state), it has been shown that secondary effects from "knockout" mutations can alter the environments of distant residues,[9] alter protein conformation independent of Ca^{2+},[8] and disrupt molecular association.[23] We also investigated the

construct “NW1-DDAA”, which combines both classes of mutations. We find that these two classes of mutations are not independent, and we show that they influence binding site properties in unintended ways that are difficult to detect by most experimental measurements.

To better understand how mutations alter ion-dependent protein structure, we need approaches that can distinguish site-resolved details of wild-type proteins from each class of mutation. CaM’s ion binding sites are rich in amino acids containing carboxylate side chains that directly coordinate Ca^{2+} (Figure 1B,D), thus providing spectroscopic reporters sensitive to ion binding. Indeed, attenuated total reflectance (ATR) Fourier transform infrared (FTIR) spectroscopy of carboxylate vibrational modes has recently been used to monitor ion binding in the MgtE magnesium channel.[24] Similarly, we use FTIR and ultrafast two-dimensional infrared (2D IR) spectroscopy of CaM’s carboxylate asymmetric stretching modes as structurally specific, mutation-free, and label-independent probes of the protein’s Ca^{2+} binding sites. The carboxylate groups are sensitive to changes in their electrostatic environment; their infrared absorptions report structural perturbations with picometer spatial sensitivity and subpicosecond temporal precision.[25–27] For example, our recent measurements of ion-dependent spectroscopic shifts[6] and vibrational lifetimes[7] in EDTA demonstrate that FTIR and 2D IR can detect structural changes induced by varying the metal ion coordination radius by <10 pm. Infrared spectroscopy of the carboxylate asymmetric stretch thus reports on conformational dynamics[2829] that are beyond the resolution of common biophysical techniques.[30–32] Our approach offers advantages over earlier studies of proteins using 2D IR that are mostly focused on interpreting the spectrum of the native amide I vibrational mode, which reports on global protein conformation and dynamics, or on using vibrational labels to probe site-specific dynamics.[33–50]

Here, we characterize the ion-dependent binding conformations of N-CaM mutants by measuring spectral signatures in the carboxylate asymmetric stretching region (1540–1600 cm^{-1}). Our interpretation of carboxylate vibrational spectra is aided by the structure of CaM’s binding sites.[51] Each site includes a single glutamate residue, which—in WT CaM—coordinates Ca^{2+} in a bidentate configuration through both carboxylate oxygens, and multiple aspartate residues that coordinate bound ions in monodentate configurations through a single carboxylate oxygen. Unbound, monodentate, and bidentate carboxylate groups each have unique spectral signatures that allow their identification and analysis through infrared spectroscopy.[52–55]

Unoccupied CaM binding sites show a single broad carboxylate asymmetric stretching feature around 1575 cm^{-1}. In Ca^{2+}-bound CaM, this feature splits into two sharper absorptions: one around 1553 cm^{-1}, which corresponds to bidentate carboxylate groups, and one around 1580 cm^{-1}, which corresponds to monodentate carboxylate groups. The 1553 cm^{-1} signature of bidentate carboxylate coordination is valuable as a spectroscopic marker of native Ca^{2+} coordination because the canonical 12th position glutamate is strongly conserved in all CaM Ca^{2+} binding sites and gives rise to a distinct spectral feature. This feature appears as a shoulder in FTIR spectra (Figure 2) and becomes better-resolved in 2D IR spectra (Figures 3 and 4). Our results thus show that 2D IR spectroscopy provides line

shapes that are sharper and better-resolved than those from FTIR, allowing for unambiguous interpretation of the spectra.

METHODS

N-CaM Mutation.

The N-terminal lobe construct (N-CaM) of vertebrate CaM (rat mRNA for Calm2, GenBank NM_017326) used in our studies terminates in D80 after the amino acid sequence KDTD. Mutation of N-CaM in the pET21a vector (Millipore Sigma) was accomplished through polymerase chain reaction of single-site mutation primers (Millipore Sigma) with the WT plasmid. The mutant plasmid so prepared was amplified in TOP10 (ThermoFisher) chemically competent cells. The primary sequence of the mutants was verified (GeneWiz) prior to expression and purification.

N-CaM Expression and Purification.

Recombinant, tagless N-CaM in the pET21a vector (Millipore Sigma) was expressed in BL21(DE3) cells (New England Biolabs). N-CaM was purified using established methods[56] but with addition of a final fractionation step using a preparative grade C18 column with an acetonitrile gradient for protein elution.

The purified N-CaM solution was flash-frozen in LN_2 and lyophilized. The lyophilized product was deuterated by incubation in pure D_2O (Cambridge Isotope Laboratories, 99.9% isotopic purity) at 50 °C for 2 h before being flash-frozen and lyophilized again. The lyophilized, deuterated CaM was finally dissolved in a 50 mM solution of deuterated MOPS in D_2O adjusted to an uncorrected pH of 6.3, which corresponds to a corrected pH reading of 6.7.[57,58] The pH was adjusted with DCl (Sigma-Aldrich, 99 atom % D) and NaOD (Sigma-Aldrich, 99 atom % D). This pH was chosen because it was found to allow both N-CaM and lanthanide salts to dissolve. Lower pH values cause N-CaM to aggregate and precipitate, while higher values cause terbium hydroxides to precipitate.

The N-CaM/MOPS solution was combined in equal proportion with solutions of anhydrous $CaCl_2$ (Sigma-Aldrich, >97%) or $TbCl_3$ (Alfa Aesar, 99.9%) in 50 mM MOPS/D_2O to yield final samples 1.1 mM in N-CaM, 2.2 mM in calcium or lanthanide ion to ensure saturation in all binding sites, and 50 mM in MOPS, in D_2O at an uncorrected pH reading of 6.3.

FTIR Spectroscopy.

FTIR spectra were measured with a Bruker Vertex 70 spectrometer with a DTGS detector at 2 cm^{-1} resolution and averaging 32 scans per spectrum. The 50 μL sample was held between two CaF_2 windows separated by a 50 μm PTFE spacer. The sample area was purged with dry (−100 °F dew point) air until no water vapor absorption lines were visible in the spectrum.

2D IR Spectroscopy.

2D IR spectra were measured with a custom-built 2D IR spectrometer as described in detail in our previous work.[6] In short, a 100 fs mid-infrared laser pulse probes the time-dependent IR absorption spectrum of the sample following excitation by a pair of pump pulses. The

excitation frequency is obtained by numerically computing the Fourier transform of the signal along the delay between the pump pulses, and the detection frequency is obtained by dispersing the probe pulse onto an infrared camera with a diffraction grating. Analogous to 2D NMR COSY, 2D IR thus spreads the IR frequency information across two axes and allows for measurement of energy transfer and vibrational relaxation.[34,38,59–62]

RESULTS

FTIR Spectroscopy.

FTIR spectra (Figure 2) show mutation- and ion-dependent changes in the line shapes of binding site carboxylate absorptions. To highlight these changes as a function of mutation, the WT apo spectrum is shown at the bottom and the WT Ca^{2+} spectrum shown at the top, as references. The signature of native bidentate glutamate Ca^{2+} binding, a shoulder around 1553 cm^{-1}, is similar in strength in the WT Ca^{2+} and NW1 Ca^{2+} spectra. This feature remains present in the DDAA Ca^{2+} spectrum but is attenuated. The bidentate glutamate signature is absent from the NW1-DDAA Ca^{2+} spectrum. Comparison of the NW1-DDAA Ca^{2+} spectrum with the WT apo spectrum shows that the two are indistinguishable within the noise level of the measurement.

2D IR Spectroscopy.

2D IR spectra (Figure 3) highlight mutation-dependent changes in carboxylate line shapes and reflect the same features reported by the FTIR spectra (Figure 2). Contour lines trace the two-dimensional spectral amplitude, with positive features denoted by red/yellow shading and negative features denoted by blue shading. Elongation of spectra along the diagonal, termed inhomogeneous broadening, yields elliptical line shapes. Such line shapes indicate the presence of multiple molecular configurations that do not interconvert during the 500 fs time scale of the measurement and thus preserve the correlation between excitation and detection frequencies. Conversely, spectral elongation perpendicular to the diagonal, termed homogeneous broadening, yields circular line shapes. These line shapes indicate interconversion of molecular configurations during the 500 fs time scale of the measurement, which scrambles excitation–detection correlation. In general, greater inhomogeneous broadening is a hallmark of conformational disorder in proteins, indicating the presence of multiple configurations that do not exchange during spectroscopic measurement. The peak amplitude of 2D IR features carries similar information: the fourth-order dependence of 2D IR amplitude upon the transition dipole, coupled with the overlap between the ground-state-bleach and excited-state absorption features, makes peak amplitude a good reporter of local heterogeneity. Heterogeneous environments produce broader peaks carrying a lower overall intensity.[63] A more detailed discussion of 2D IR data collection and analysis is available in a previous publication.[6]

The apo spectra of WT and all mutants (top row) appear similar and are without clear bidentate glutamate coordination signatures around 1553 cm^{-1}. The Ca^{2+} spectra (middle row) show strong bidentate glutamate coordination signatures for both WT and NW1. The DDAA spectrum shows weaker absorption in this region. The NW1-DDAA spectrum does not show bidentate glutamate absorption and is comparable to the apo spectrum. The Tb^{3+}

spectra (bottom row) for WT, NW1, and DDAA show the red-shifted carboxylate features associated with lanthanide coordination near 1535 cm^{-1}.[6] This feature appears to be red-shifted and to have a narrower inhomogeneous line width in the DDAA mutant than in WT or the NW1 mutant. Signs of Tb^{3+} coordination are not clear in spectra of the NW1-DDAA mutant.

Diagonal slices (Figure 4) extracted from the full 2D IR spectra highlight mutant-dependent spectral changes and serve as a point of comparison between FTIR spectra (Figure 2) and the corresponding 2D IR data. The 2D IR slices show mutant to mutant changes that essentially mirror those reported by FTIR, but peaks are narrower and better resolved. The NW1-DDAA Ca^{2+} spectrum closely matches the WT apo spectrum: both show no bidentate glutamate peaks. The growth of a small bidentate glutamate signal is visible in the DDAA slice as a separate peak, as opposed to the weak shoulder visible in the FTIR spectra. The 2D IR spectra thus reveal features that are more difficult to resolve using FTIR. Similar to the FTIR spectra, the 2D IR slice spectra show strong bidentate glutamate features in the NW1 and WT spectra, but the NW1 monodentate carboxylate region shows a high-frequency shoulder appearing alongside the principal band that is not observed in the FTIR spectrum.

Difference spectra (Figure 5) are extracted from the 2D IR data (Figure 3) by subtracting the apo spectrum from the Ca^{2+} and Tb^{3+} spectra of each mutant. The difference spectra thus highlight specific spectral signatures of Ca^{2+} and Tb^{3+} binding relative to the unbound protein. Red/yellow features in the difference spectra signify an increase, and blue features a decrease, in spectral amplitude going from the unbound structure to the bound structure. As seen in the previous results, the Ca^{2+} – apo difference spectra (top row) show a decrease in growth of the bidentate glutamate peak as the protein structure is changed from WT to NW1 to DDAA to NW1-DDAA The difference spectra offer insights in addition to those provided by the preceding data. (i) A decrease in the amplitude of the bidentate glutamate peak is visible between WT and NW1, and (ii) there is a weak but measurable bidentate glutamate feature in the NW1-DDAA spectrum. Examination of the Tb^{3+} – apo difference spectra (bottom row) shows growth in the carboxylate lanthanide coordination peak for the WT and NW1 structures. The DDAA and NW1-DDAA results are more complex. The DDAA spectrum shows growth of both the lanthanide coordination feature around 1535 cm^{-1} and a more intense, higher-frequency feature in the carboxylate region centered around 1580 cm^{-1}. The NW1-DDAA spectrum shows growth of a broad, diagonally elongated band spanning the entire frequency range of 1540–1590 cm^{-1}.

DISCUSSION

Effects of Mutation on Ca^{2+} Binding by N-CaM.

CaM has multiple metal binding sites. Determining equilibrium constants from binding data presents real challenges, and interpretations of complete occupancy depend on whether a curve reaches saturation.[4,64–67] Multiple groups have shown that WT CaM's N lobe, whether isolated or part of full-length CaM, reaches half-saturation at around 6 μM Ca^{2+}[5,11,20,68,69] and at much lower Tb^{3+} concentrations.[70–72] In addition, the NW1 mutation does not appreciably alter Ca^{2+} binding.[5] Thus, both WT N-CaM and NW1 should be fully

occupied at millimolar concentrations of protein with an exactly 2-fold molar excess of either Ca^{2+} or Tb^{3+}.

Mutation of binding site aspartate residues to alanine substantially weakens CaM's ability to bind Ca^{2+}, with no detectable binding at hundreds of micromolar Ca^{2+}.[18] Other studies using similar binding site mutations detected binding only at millimolar concentrations of Ca^{2+}, but dissociation constants for the disrupted sites were not reported.[15–17,20,73] There are also species differences in protein sequences of the calmodulins in many of these studies that include yeast,[18] insect,[20] and paramecia[68] compared to the vertebrate CaM used in our work. Thus, assessing the quantitative occupancy of the DDAA mutant CaM under our experimental conditions is problematic, and any estimate we can make is at best semiquantitative. What is clear is that the DDAA mutation significantly disrupts Ca^{2+} binding, but some occupancy of the sites at millimolar protein and metal ion concentrations is possible. Although occupancy of the disrupted sites is hard to quantify, knowing the exact occupancy is not necessary to interpret our 2D IR results. The 2D IR data contain broad featural changes that are qualitatively informative with our approach and provide structural insights not available from other methods. Examination of the 2D IR spectra (Figure 3), diagonal slices (Figure 4), and difference spectra (Figure 5) reveals the nuanced structural perturbations to the binding sites that accompany mutation.

Several observations set a foundation for comparing ion binding to the different protein constructs. (i) From Figure 3, we see that 2D IR spectra vary with both ion and protein mutation. Although there are some broad similarities, there are also important differences that can be elucidated by different views of these data sets. These data can be analyzed more closely by looking at diagonal slices (Figure 4) and difference spectra (Figure 5). (ii) From Figure 4, we learn that although both WT and NW1 have similar overall spectral profiles, they are not the same. The NW1 spectrum is broader and includes a shoulder around 1590 cm^{-1} that is indicative of multiple monodentate configurations, a sign of greater structural heterogeneity in NW1. Greater differences are seen in constructs with the DDAA mutations. The intensities of the bidentate features of DDAA and NW1-DDAA at 1553 cm^{-1} are 34% and <2%, respectively, of that of the WT (Table 1), indicating a reduction in bidentate ion coordination. (iii) From the difference spectra in Figure 5, we learn that distinctions between WT and NW1 are small compared with the greater distortions caused by the DDAA mutations, especially in the presence of Tb^{3+}.

Modulation of the bidentate peak in FTIR and 2D IR spectra suggests that Ca^{2+} binding in the NW1 mutant is similar to that of WT in agreement with previous studies. However, our infrared spectra indicate that the DDAA mutant has a limited effect on binding site structure, despite the reported disruption to binding. Clear signatures of bidentate binding appear in the DDAA spectrum (Table 1). Perhaps the observed effect of Ca^{2+} on DDAA is unsurprising given that the experiments were performed at millimolar protein and ion concentrations where some binding of Ca^{2+} to mutants with site disruptions might be expected.[15,73]

These results indicate that the NW1 and DDAA mutations have effects beyond their designed purposes. The NW1 mutant, rather than leaving binding site structure undisturbed,

reduces the population of bidentate glutamates and introduces an additional, non-native monodentate carboxylate configuration. Similarly, the DDAA mutant attenuates signatures of native binding. Therefore, the NW1 and DDAA mutants achieve effects similar to those expected but at the cost of unintended side effects that are not detected by other measurements. Furthermore, the attenuation of the bidentate peak and simultaneous broadening of the monodentate band that accompanies mutation suggest a more heterogeneous structural ensemble in N-CaM mutants, in contrast to the well-defined configuration of the WT protein.

Our interpretations are limited to the isolated N lobe of CaM in solution. The C lobe of CaM may influence the binding of Ca^{2+} to the N lobe through cooperative interactions. Prior studies suggest that single-lobe versus full-length CaM peptides may behave differently. For example, in the presence of a CaM binding partner, binding of Ca^{2+} to the N lobe of CaM is sensitive to whether it is isolated or part of a full-length protein.[74,75] Additionally, the length of the N lobe protein construct, even without a partner, can contribute to both protein thermostability and Ca^{2+} affinity.[76] Our vertebrate N-CaM protein construct ending in residues DTD matched the longer and more thermostable equivalent Paramecium construct ending with residues EQD, which behaved essentially like full-length CaM in another study.[76] More sophisticated efforts are needed to determine whether the C lobe of CaM could further alter the N lobe signatures in the 2D IR spectra because Ca^{2+}-coordinating carboxylates are also present in the C lobe.

Effects of Mutation on Tb^{3+} Binding by N-CaM.

Our previous study of binding in full-length, WT CaM shows that binding of lanthanide ions in place of Ca^{2+} causes CaM's binding sites to contract, undergoing a transition from the well-ordered and rapidly exchanging manifold characteristic of native binding configurations to an ensemble of disordered and more static lanthanide-bound configurations.[6] 2D IR difference spectra of the N-CaM mutants in this study (Figure 5) extend this description of perturbed binding site structure. The results indicate that Tb^{3+} binding by the NW1 mutant is similar to that of the WT, but the decreased diagonal line width in the NW1 Tb^{3+} – apo difference spectrum relative to WT suggests that the Tb^{3+}-occupied mutant site is less disordered. Difference spectra of the Tb^{3+}-bound DDAA and NW1-DDAA mutants show especially interesting features. In the DDAA spectrum, the increased intensity around 1575 cm^{-1}, in addition to the expected lanthanide coordination signature around 1535 cm^{-1}, indicates the presence of strong, mutation-dependent monodentate or pseudobridging (one oxygen binds a metal, while the other oxygen forms a hydrogen bond to water) carboxylate configurations unique to the Tb^{3+}-bound DDAA mutant. The well-defined features present in WT, NW1, and DDAA spectra are absent in the NW1-DDAA spectrum and are replaced by an inhomogeneously broadened feature spanning the entire range of 1540–1590 cm^{-1}, suggesting that the Tb^{3+}-bound NW1-DDAA site occupies a more heterogeneous conformational ensemble. Therefore, Tb^{3+} binds the DDAA and NW1-DDAA sites in unique, structurally disordered configurations that differ from the WT and NW1 Tb^{3+}-bound structures. The NW1-DDAA site shows especially strong spectral markers of structural disorder.

Comparison of Binding of Ca^{2+} and Tb^{3+} by N-CaM Mutants.

Similarity of WT and NW1 Sites.—Comparison of 2D IR difference spectra for WT and NW1 N-CaM (Figure 5, leftmost four spectra) suggests that binding of Ca^{2+} and Tb^{3+} is similar across these structures. In all four spectra, ion binding induces the growth of a single homogeneous feature in the bidentate region of the spectrum. Due to the broader spectral line width arising from the greater conformational heterogeneity of the Tb^{3+}-occupied sites, these features are weaker in the WT and NW1 Tb^{3+} – apo difference spectra than in the corresponding Ca^{2+} – apo difference spectra.

Distinctions between the DDAA and NW1-DDAA Sites.—The pattern described above does not hold in the DDAA and NW1-DDAA mutants, where the Tb^{3+} – apo difference spectra show more pronounced differences, namely, more intense peaks and broader features, than their Ca^{2+} – apo counterparts. These changes suggest that Tb^{3+} binds the DDAA and NW1-DDAA mutants with greater disorder and a more contracted coordination structure than it does the WT or NW1 proteins. Notably, the DDAA and NW1-DDAA mutations introduce structural disorder beyond that characteristic of the Tb^{3+}-bound WT site, which is already disordered relative to the Ca^{2+}-bound WT site.[6] Finally, comparison of the WT and NW1-DDAA difference spectra shows that the NW1-DDAA Ca^{2+} – apo carboxylate growth band is ~10 times weaker than its WT Ca^{2+} – apo counterpart, while the NW1-DDAA and WT Tb^{3+} – apo carboxylate growth bands are of comparable strength. The DDAA and NW1-DDAA mutations thus create unique binding modes, with contracted binding sites and increased structural heterogeneity, that are capable of binding Tb^{3+} but not Ca^{2+}. The presence of these binding modes allows the DDAA and NW1-DDAA mutants to bind Tb^{3+} even though their Ca^{2+} affinities are reduced.[18]

Modulation of the Conformational Landscape by Mutagenesis.

Our results show that the NW1 mutation induces small, but measurable, modulations to the N-CaM Ca^{2+} binding structure and that the DDAA mutation attenuates Ca^{2+} binding signatures by ~50%. Assuming that there is little communication between the NW1 and DDAA mutations, one would expect the NW1-DDAA Ca^{2+} – apo difference spectrum to resemble the DDAA Ca^{2+} – apo difference spectrum because the NW1 mutation seems to cause an only minor change to the binding site. However, difference spectra (Figure 5) of the NW1-DDAA mutant bound to Ca^{2+} and Tb^{3+} are clearly distinct from all other spectra. The NW1-DDAA Tb^{3+} – apo difference spectrum is marked by greater inhomogeneous broadening than any other spectrum, and the NW1-DDAA Ca^{2+} – apo difference spectrum is characterized by carboxylate region growth features <30% as intense as the next-weakest spectrum (DDAA). Signs of Ca^{2+} binding in the NW1-DDAA mutant, which are clear in all other cases, are only marginally above the noise floor in the 2D IR difference spectrum (Figure 5) and are not visible in any of the other data.

This result indicates that the NW1 and DDAA mutations modify the free energy surface of the binding site along coordinates that are not probed by our spectroscopic methods. These changes alter the conformational landscape of the mutant but become apparent only when an additional perturbation is made. For example, the NW1 mutation alone has only minor effects on the binding site vibrational spectrum but causes clear spectral changes when

introduced into the DDAA mutant. A plausible explanation is that the NW1 mutation alters N-CaM's free energy surface in a way that makes the protein's binding site configuration less robust against the DDAA mutation without inducing major structural changes to the binding site. This effect is not clear in the NW1 spectrum but is immediately obvious in the comparison between the DDAA and NW1-DDAA results.

Therefore, the results argue for the presence of mutagenesis-driven modulations to the conformational landscape that are difficult to measure in the absence of further perturbation. This result is significant because CaM does not act alone but in combination with a wide variety of ion channels and other effector proteins, each of which interacts with and influences CaM differently.[77] Mutations or other perturbations to protein structure whose effects are apparently negligible under a particular set of conditions may behave differently as conditions are changed and different regions of CaM's conformational topology become relevant.

Comparison of FTIR Spectra with 2D IR Ground-State-Bleach Slices.

FTIR (Figure 2) and 2D IR slice (Figure 4) spectra both show that the signatures of native Ca^{2+} binding in N-CaM gradually disappear upon proceeding from WT toward NW1, DDAA, and NW1-DDAA However, direct comparison of Figures 2 and 4 shows that the 2D IR slice spectra offer discrete spectral features for analysis in place of the broad envelopes provided by FTIR. These more structured spectra make it possible to better resolve and quantify spectral differences, such as changes to the amplitude of the bidentate carboxylate bands and the appearance of weak structure in the NW1 Ca^{2+} carboxylate spectrum. This distinction is typical of the spectral narrowing and background suppression offered by 2D IR spectroscopy,[35] where the signal amplitude varies with the transition dipole moment (μ) as μ^4, in contrast to the μ^2 dependence characteristic of linear spectroscopies such as FTIR. This feature of 2D IR spectroscopy serves to enhance sharper features such as the carboxylate peaks while suppressing broader features, such as the solvent background and amide I modes.[41] Therefore, 2D IR spectroscopy and other nonlinear optical spectroscopies are particularly effective tools for probing complex molecular structures, such as proteins, that give rise to broad and complex spectral line shapes.

CONCLUSION AND OUTLOOK

Binding of a series of N-CaM mutants to Ca^{2+} and Tb^{3+} was studied with FTIR and ultrafast 2D IR spectroscopy. We found that mutations that are designed and commonly used to introduce chromophores within, or to selectively disrupt, CaM's binding sites exerted additional, unintended effects on those sites.

Experimental findings include the following. (i) The native Ca^{2+} binding structure is subtly altered by the NW1 mutation, disrupted by the DDAA mutation, and severely disrupted by the NW1-DDAA mutation. These structural effects are evident in the similarity of the 2D line shapes in the Ca^{2+}-bound WT and NW1 spectra, which appear to be different than the corresponding DDAA and NW1-DDAA spectra. (ii) Tb^{3+}-bound sites in the NW1 mutant and WT proteins are similar, while those in the DDAA and NW1-DDAA mutants are structurally disordered. These conclusions are supported by the similar peak positions and

diagonal line widths shown by the Tb^{3+}-bound WT and NW1 proteins, which are markedly distinct from the inhomogeneously broadened line shapes of the Tb^{3+}-bound DDAA and NW1-DDAA mutants. (iii) The presence of structurally disordered Tb^{3+} binding configurations allows the DDAA and NW1-DDAA mutants to bind Tb^{3+} despite disruption of native Ca^{2+} binding. Strong, diagonally broadened markers of Tb^{3+} coordination are present in the DDAA and NW1-DDAA spectra, while markers of Ca^{2+} binding are greatly attenuated in these mutants. (iv) The NW1 mutation introduces changes to N-CaM's free energy landscape along coordinates that cannot be probed by our methods and become measurable only in the presence of additional structural perturbation, such as the DDAA mutation. These changes are suggested by the differences between the spectra of the DDAA and NW1-DDAA mutants, which are much clearer than those between the WT and NW1 pair even though each pair is separated by the same NW1 mutation. (v) Comparison of FTIR line shapes with ground-state-bleach slices taken from the 2D IR spectra demonstrates the advantages offered by 2D IR spectroscopy for the study of protein biophysics.

Taken together, the findings demonstrate that binding site mutations may introduce unintended effects that are difficult to predict. Furthermore, these effects communicate by changing N-CaM's conformational landscape in ways that are challenging to measure with conventional techniques. This result has implications for the study of CaM and other signaling proteins because useful mutations that seem nonperturbative under one set of conditions may exhibit divergent behavior under another. The effects of complex and fluctuating molecular environments on the free energy landscape are especially important in biological systems, where the concentrations of a wide range of competitively binding ions change frequently and rapidly in response to signaling events.

The results also show that the NW1, DDAA, and NW1-DDAA mutations affect Ca^{2+} and Tb^{3+} binding differently. For example, binding of Ca^{2+} to the NW1-DDAA mutant is nearly eliminated, yet the mutan's capacity to bind Tb^{3+} remains intact. Furthermore, large differences in binding site structure separate the Tb^{3+}-bound NW1-DDAA mutant and its WT counterpart even though they both appear to bind Tb^{3+}. As such, changes in binding competence and binding structure depend on both mutation and bound ion but do not track predictably with either parameter or with one another.

Infrared spectroscopy offers a sensitive, physically direct probe of binding site structure. Our results reveal additional complexities in the conformational landscape produced by modulating protein structure through mutagenesis and ion binding. In addition, they demonstrate the utility of infrared spectroscopy for mapping unexplored regions of this landscape.

Supplementary Material

Refer to Web version on PubMed Central for supplementary material.

ACKNOWLEDGMENTS

Computer simulations were run at the Texas Advanced Computing Center.

Funding

The authors gratefully acknowledge financial support from the College of Natural Sciences at The University of Texas at Austin for seed funding through a Catalyst Grant, from the Welch Foundation under Grant F-1891, from the National Institutes of Health under Grant R01NS077821, and from the National Science Foundation under Grant BIO-1815354.

REFERENCES

(1). Forsen S, and Lindman B (1981) In Ion binding in biological systems as studied by NMR spectroscopy (Glick D, Ed.) Chapter 5, pp 289–486, John Wiley & Sons.

(2). Petukh M, and Alexov E (2014) Ion binding to biological macromolecules. Asian J. Phys 23, 735. [PubMed: 25774076]

(3). Roux B, Allen T, Berneche S, and Im W (2004) Theoretical and computational models of biological ion channels. Q. Rev. Biophys 37, 15–103. [PubMed: 17390604]

(4). Middendorf TR, and Aldrich RW (2017) Structural identifiability of equilibrium ligand-binding parameters. J. Gen. Physiol 149, 105–119. [PubMed: 27993952]

(5). Kilhoffer MC, Kubina M, Travers F, and Haiech J (1992) Use of engineered proteins with internal tryptophan reporter groups and perturbation techniques to probe the mechanism of ligand-protein interactions: investigation of the mechanism of calcium binding to calmodulin. Biochemistry 31, 8098–8106. [PubMed: 1510991]

(6). Edington SC, Gonzalez A, Middendorf TR, Halling DB, Aldrich RW, and Baiz CR (2018) Coordination to lanthanide ions distorts binding site conformation in calmodulin. Proc. Natl. Acad. Sci. U. S. A 115, E3126–E3134. [PubMed: 29545272]

(7). Edington SC, and Baiz CR (2018) Vibrational Relaxation in EDTA Is Ion-Dependent. J. Phys. Chem. A 122, 6585–6592. [PubMed: 30024164]

(8). Piazza M, Taiakina V, Dieckmann T, and Guillemette JG (2017) Structural consequences of calmodulin EF hand mutations. Biochemistry 56, 944–956. [PubMed: 28121131]

(9). Xiong L-W, Kleerekoper QK, Wang X, and Putkey JA (2010) Intra and interdomain effects due to mutation of calcium binding sites in calmodulin. J. Biol. Chem 285, 8094. [PubMed: 20048169]

(10). Persechini A, McMillan K, and Leakey P (1994) Activation of myosin light chain kinase and nitric oxide synthase activities by calmodulin fragments. J. Biol. Chem 269, 16148–16154. [PubMed: 7515878]

(11). Linse S, Helmersson A, and Forsen S (1991) Calcium binding to calmodulin and its globular domains. J. Biol. Chem 266, 8050–8054. [PubMed: 1902469]

(12). Halling DB, Liebeskind BJ, Hall AW, and Aldrich RW (2016) Conserved properties of individual Ca^{2+}-binding sites in calmodulin. Proc. Natl. Acad. Sci. U. S. A 113, E1216–E1225. [PubMed: 26884197]

(13). Black D, Tikunova SB, Johnson JD, and Davis JP (2000) Acid pairs increase the N-terminal Ca^{2+} affinity of CaM by increasing the rate of Ca^{2+} association. Biochemistry 39, 13831–13837. [PubMed: 11076523]

(14). Drake SK, Lee KL, and Falke JJ (1996) Tuning the equilibrium ion affinity and selectivity of the EF-hand calcium binding motif: substitutions at the gateway position. Biochemistry 35, 66976705.

(15). Mukherjea P, Maune JF, and Beckingham K (1996) Interlobe communication in multiple calcium-binding site mutants of Drosophila calmodulin. Protein Sci. 5, 468–477. [PubMed: 8868483]

(16). Maune J, Klee C, and Beckingham K (1992) Ca^{2+} binding and conformational change in two series of point mutations to the individual Ca^{2+}-binding sites of calmodulin. J. Biol. Chem. 267, 52865295.

(17). Martin SR, Maune JF, Beckingham K, and Bayley PM (1992) Stopped-flow studies of calcium dissociation from calcium-binding-site mutants of Drosophila melanogaster calmodulin. Eur. J. Biochem 205, 1107–1117. [PubMed: 1576994]

(18). Geiser JR, van Tuinen D, Brockerhoff SE, Neff MM, and Davis TN (1991) Can calmodulin function without binding calcium? Cell 65, 949–959. [PubMed: 2044154]

(19). Evenäs J, Malmendal A, Thulin E, Carlström G, and Forsén S (1998) Ca^{2+} binding and conformational changes in a calmodulin domain. Biochemistry 37, 13744–13754. [PubMed: 9753463]

(20). Beckingham K (1991) Use of site-directed mutations in the individual Ca^{2+}binding sites of calmodulin to examine Ca^{2+}-induced conformational changes. J. Biol. Chem 266, 6027–6030. [PubMed: 1901056]

(21). Putkey JA, Sweeney HL, and Campbell S (1989) Site-directed mutation of the trigger calcium-binding sites in cardiac troponin C. J. Biol. Chem 264, 12370–12378.

(22). Xia X-M, Fakler B, Rivard A, Wayman G, Johnson-Pais T, Keen J, Ishii T, Hirschberg B, Bond C, Lutsenko S, et al. (1998) Mechanism of calcium gating in small-conductance calcium-activated potassium channels. Nature 395, 503. [PubMed: 9774106]

(23). Li W, Halling DB, Hall AW, and Aldrich RW (2009) EF hands at the N-lobe of calmodulin are required for both SK channel gating and stable SK-calmodulin interaction. J. Gen. Physiol 134, 281–293. [PubMed: 19752189]

(24). Kimura T, Lorenz-Fonfria VA, Douki S, Motoki H, Ishitani R, Nureki O, Higashi M, and Furutani Y (2018) Vibrational and molecular properties of Mg^{2+} binding and ion selectivity in the magnesium channel MgtE. J. Phys. Chem. B 122, 9681–9696. [PubMed: 30252477]

(25). Abaskharon RM, Brown SP, Zhang W, Chen J, Smith AB, and Gai F (2017) Isotope-labeled aspartate sidechain as a non-perturbing infrared probe: application to investigate the dynamics of a carboxylate buried inside a protein. Chem. Phys. Lett 683, 193–198. [PubMed: 29033461]

(26). Slayton RM, and Anfinrud PA (1997) Time-resolved mid-infrared spectroscopy: methods and biological applications. Curr. Opin. Struct. Biol 7, 717–721. [PubMed: 9345632]

(27). Callender R, and Dyer RB (2006) Advances in time-resolved approaches to characterize the dynamical nature of enzymatic catalysis. Chem. Rev 106, 3031–3042. [PubMed: 16895316]

(28). Kuroda DG, Vorobyev DY, and Hochstrasser RM (2010) Ultrafast relaxation and 2D IR of the aqueous trifluorocarboxylate ion. J. Chem. Phys 132, 044501. [PubMed: 20113043]

(29). Banno M, Ohta K, and Tominaga K (2008) Ultrafast dynamics of the carbonyl stretching vibration in acetic acid in aqueous solution studied by sub-picosecond infrared spectroscopy. J. Phys. Chem. A 112, 4170–4175. [PubMed: 18373362]

(30). Markwick PR, Malliavin T, and Nilges M (2008) Structural biology by NMR: structure, dynamics, and interactions. PLoS Comput. Biol 4, e1000168. [PubMed: 18818721]

(31). Shi Y (2014) A glimpse of structural biology through X-ray crystallography. Cell 159, 995–1014. [PubMed: 25416941]

(32). Henzler-Wildman K, and Kern D (2007) Dynamic personalities of proteins. Nature 450, 964–972. [PubMed: 18075575]

(33). Wang L, Middleton CT, Singh S, Reddy AS, Woys AM, Strasfeld DB, Marek P, Raleigh DP, de Pablo JJ, Zanni MT, et al. (2011) 2DIR spectroscopy of human amylin fibrils reflects stable β-sheet structure. J. Am. Chem. Soc 133, 16062–16071. [PubMed: 21916515]

(34). Petti MK, Lomont JP, Maj M, and Zanni MT (2018) Two-Dimensional Spectroscopy Is Being Used to Address Core Scientific Questions in Biology and Materials Science. J. Phys. Chem. B 122, 1771–1780. [PubMed: 29346730]

(35). Middleton CT, Marek P, Cao P, Chiu C. c., Singh S, Woys AM, De Pablo JJ, Raleigh DP, and Zanni MT (2012) Two-dimensional infrared spectroscopy reveals the complex behaviour of an amyloid fibril inhibitor. Nat. Chem 4, 355–360. [PubMed: 22522254]

(36). Thielges MC, Axup JY, Wong D, Lee HS, Chung JK, Schultz PG, and Fayer MD (2011) Two-dimensional IR spectroscopy of protein dynamics using two vibrational labels: a site-specific genetically encoded unnatural amino acid and an active site ligand. J. Phys. Chem. B 115, 11294–11304. [PubMed: 21823631]

(37). Remorino A, and Hochstrasser RM (2012) Three-dimensional structures by two-dimensional vibrational spectroscopy. Acc. Chem. Res 45, 1896–1905. [PubMed: 22458539]

(38). Kim YS, and Hochstrasser RM (2009) Applications of 2D IR spectroscopy to peptides, proteins, and hydrogen-bond dynamics. J. Phys. Chem. B 113, 8231–8251. [PubMed: 19351162]

(39). Le Sueur AL, Horness RE, and Thielges MC (2015) Applications of two-dimensional infrared spectroscopy. Analyst 140, 4336–4349. [PubMed: 26007625]

(40). Serrano AL, Waegele MM, and Gai F (2012) Spectroscopic studies of protein folding: linear and nonlinear methods. Protein Sci 21, 157–170. [PubMed: 22109973]

(41). Baiz CR, Reppert M, and Tokmakoff A (2013) An Introduction to Protein 2D IR Spectroscopy. In Ultrafast Infrared Vibrational Spectroscopy (Fayer MD, Ed.) pp 361–404, Taylor & Francis, New York.

(42). Minnes L, Shaw DJ, Cossins BP, Donaldson PM, Greetham GM, Towrie M, Parker AW, Baker MJ, Henry AJ, Taylor RJ, et al. (2017) Quantifying Secondary Structure Changes in Calmodulin Using 2D-IR Spectroscopy. Anal. Chem 89, 10898–10906. [PubMed: 28921967]

(43). Kratochvil HT, Carr JK, Matulef K, Annen AW, Li H, Maj M, Ostmeyer J, Serrano AL, Raghuraman H, Moran SD, et al. (2016) Instantaneous ion configurations in the K^+ ion channel selectivity filter revealed by 2D IR spectroscopy. Science 353, 1040–1044. [PubMed: 27701114]

(44). Kelly KL, Dalton SR, Wai RB, Ramchandani K, Xu RJ, Linse S, and Londergan CH (2018) Conformational Ensembles of Calmodulin Revealed by Nonperturbing Site-Specific Vibrational Probe Groups. J. Phys. Chem. A 122, 2947–2955. [PubMed: 29400461]

(45). Xu RJ, Blasiak B, Cho M, Layfield JP, and Londergan CH (2018) A Direct, Quantitative Connection between Molecular Dynamics Simulations and Vibrational Probe Line Shapes. J. Phys. Chem. Lett 9, 2560–2567. [PubMed: 29697984]

(46). Kratochvil HT, Maj M, Matulef K, Annen AW, Ostmeyer J, Perozo E, Roux B, Valiyaveetil FI, and Zanni MT (2017) Probing the Effects of Gating on the Ion Occupancy of the K+ Channel Selectivity Filter Using Two-Dimensional Infrared Spectroscopy. J. Am. Chem. Soc 139, 8837–8845. [PubMed: 28472884]

(47). van Wilderen LJ, Kern-Michler D, Muller-Werkmeister HM, and Bredenbeck J (2014) Vibrational dynamics and solvatochromism of the label SCN in various solvents and hemoglobin by time dependent IR and 2D-IR spectroscopy. Phys. Chem. Chem. Phys 16, 19643–19653. [PubMed: 25111557]

(48). Ma J, Pazos IM, Zhang W, Culik RM, and Gai F (2015) Site-specific infrared probes of proteins. Annu. Rev. Phys. Chem 66, 357–377. [PubMed: 25580624]

(49). Chalyavi F, Hogle DG, and Tucker MJ (2017) Tyrosine as a non-perturbing site-specific vibrational reporter for protein dynamics. J. Phys. Chem. B 121 , 6380–6389. [PubMed: 28590738]

(50). Blasiak B, Londergan CH, Webb LJ, and Cho M (2017) Vibrational probes: from small molecule solvatochromism theory and experiments to applications in complex systems. Acc. Chem. Res 50, 968–976. [PubMed: 28345879]

(51). Babu YS, Bugg CE, and Cook WJ (1988) Structure of calmodulin refined at 2.2 A resolution. J. Mol. Biol 204, 191–204. [PubMed: 3145979]

(52). Deacon G, Huber F, and Phillips R (1985) Diagnosis of the nature of carboxylate coordination from the direction of shifts of carbon-oxygen stretching frequencies. Inorg. Chim. Acta 104, 41–45.

(53). Nara M, Tasumi M, Tanokura M, Hiraoki T, Yazawa M, and Tsutsumi A (1994) Infrared studies of interaction between metal ions and Ca^{2+}-binding proteins Marker bands for identifying the types of coordination of the side-chain COO^-groups to metal ions in pike parvalbumin (pI= 4.10). FEBS Lett. 349, 84–88. [PubMed: 8045307]

(54). Yumoto F, Nara M, Kagi H, Iwasaki W, Ojima T, Nishita K, Nagata K, and Tanokura M (2001) Coordination structures of Ca^{2+} and Mg^{2+} in Akazara scallop troponin C in solution. Eur. J. Biochem. 268, 6284–6290. [PubMed: 11733025]

(55). DePalma JW, Kelleher PJ, Tavares LC, and Johnson MA (2017) Coordination-Dependent Spectroscopic Signatures of Divalent Metal Ion Binding to Carboxylate Head Groups: H2-and He-Tagged Vibrational Spectra of M^{2+}-RCO_2^- (M=Mg and Ca, R=$-CD_3$, $-CD_2CD_3$) Complexes. J. Phys. Chem. Lett 8, 484–488. [PubMed: 28060510]

(56). Marshak DR, Kadonaga JT, Burgess RR, Knuth MW, Brennan W Jr., and Lin S-H (1996) Strategies for protein purification and characterization: a laboratory course manual, Cold Spring Harbor Laboratory Press, Plainview, NY.

(57). Rubinson KA (2017) Practical corrections for p (H, D) measurements in mixed H_2O/D_2O biological buffers. Anal. Methods 9, 2744–2750.

(58). Covington AK, Paabo M, Robinson RA, and Bates RG (1968) Use of the glass electrode in deuterium oxide and the relation between the standardized pD (paD) scale and the operational pH in heavy water. Anal. Chem 40, 700–706.

(59). Fayer MD (2013) Ultrafast Infrared Vibrational Spectroscopy, Vol. 2, p 487, CRC Press, Boca Raton, FL.

(60). Hamm P, Lim M, and Hochstrasser RM (1998) Structure of the Amide-I band of peptides measured by FS nonlinear infrared spectroscopy. J. Phys. Chem. B 102, 6123.

(61). Adamczyk K, Simpson N, Greetham GM, Gumiero A, Walsh MA, Towrie M, Parker AW, and Hunt NT (2015) Ultrafast infrared spectroscopy reveals water-mediated coherent dynamics in an enzyme active site. Chem. Sci 6, 505–516. [PubMed: 28936306]

(62). Liang C, Kwak K, and Cho M (2017) Revealing the solvation structure and dynamics of carbonate electrolytes in lithiumion batteries by two-dimensional infrared spectrum modeling. J. Phys. Chem. Lett 8, 5779–5784. [PubMed: 29131650]

(63). Buchanan LE, Dunkelberger EB, Tran HQ Cheng P.-n., Chiu C.-c., Cao P, Raleigh DP, de Pablo JJ, Nowick JS, and Zanni MT (2013) Mechanism of LAPP amyloid fibril formation involves an intermediate with a transient β-sheet. Proc. Natl. Acad. Sci. U. S. A 110, 19285–19290. [PubMed: 24218609]

(64). Middendorf T, and Aldrich R (2017) The structure of binding curves and practical identifiability of equilibrium ligand-binding parameters. J. Gen. Physiol 149, 121–147. [PubMed: 27993951]

(65). Hines KE, Middendorf TR, and Aldrich R W. (2014) Determination of parameter identifiability in nonlinear biophysical models: A Bayesian approach. J. Gen. Physiol 143, 401–416. [PubMed: 24516188]

(66). Kilhoffer M, Roberts D, Adibi A, Watterson D, and Haiech J (1988) Investigation of the mechanism of calcium binding to calmodulin. Use of an isofunctional mutant with a tryptophan introduced by site-directed mutagenesis. J. Biol. Chem 263, 17023–17029. [PubMed: 3182830]

(67). Klotz IM (1985) Ligand-receptor interactions: facts and fantasies. Q. Rev. Biophys. 18, 227–259. [PubMed: 3916127]

(68). VanScyoc WS, and Shea MA (2001) Phenylalanine fluorescence studies of calcium binding to N-domain fragments of Paramecium calmodulin mutants show increased calcium affinity correlates with increased disorder. Protein Sci. 10, 1758–1768. [PubMed: 11514666]

(69). Pedigo S, and Shea MA (1995) Discontinuous equilibrium titrations of cooperative calcium binding to calmodulin monitored by 1-D 1H-nuclear magnetic resonance spectroscopy. Biochemistry 34, 10676–10689. [PubMed: 7654722]

(70). Kilhoffer MC, Demaille JG, and Gerard D (1980) Terbium as luminescent probe of calmodulin calcium-binding sites; domains L and LL contain the high-affinity sites. FEBS Lett. 116, 269–272. [PubMed: 7409149]

(71). Wang CLA, Leavis PC, and Gergely J (1984) Kinetic studies show that calcium and terbium have different binding preferences toward the four calcium-binding sites of calmodulin. Biochemistry 23, 6410–6415. [PubMed: 6529556]

(72). Wallace R, Tallant E, Dockter M, and Cheung W (1982) Calcium binding domains of calmodulin. Sequence of fill as determined with terbium luminescence. J. Biol. Chem 257, 1845–1854. [PubMed: 6276400]

(73). Zhu T, Beckingham K, and Ikebe M (1998) High affinity Ca^{2+} binding sites of calmodulin are critical for the regulation of myosin Iβ motor function. J. Biol. Chem. 273, 20481–20486. [PubMed: 9685403]

(74). Evans TLA, and Shea MA (2009) Energetics of calmodulin domain interactions with the calmodulin binding domain of CaMKII. Proteins: Struct., Funct., Genet 76, 47–61. [PubMed: 19089983]

(75). Newman RA, Van Scyoc WS, Sorensen BR, Jaren OR, and Shea MA (2008) Interdomain cooperativity of calmodulin bound to melittin preferentially increases calcium affinity of sites L and LL. Proteins: Struct., Funct. Genet 71, 1792–1812. [PubMed: 18175310]

(76). Faga LA, Sorensen BR, VanScyoc WS, and Shea MA (2003) Basic Interdomain boundary residues in calmodulin decrease calcium affinity of sites I and II by stabilizing helix–helix interactions. Proteins: Struct., Funct., Genet 50, 381–391. [PubMed: 12557181]

(77). Saimi Y, and Kung C (2002) Calmodulin as an ion channel subunit. Annu. Rev. Physiol 64, 289–311. [PubMed: 11826271]

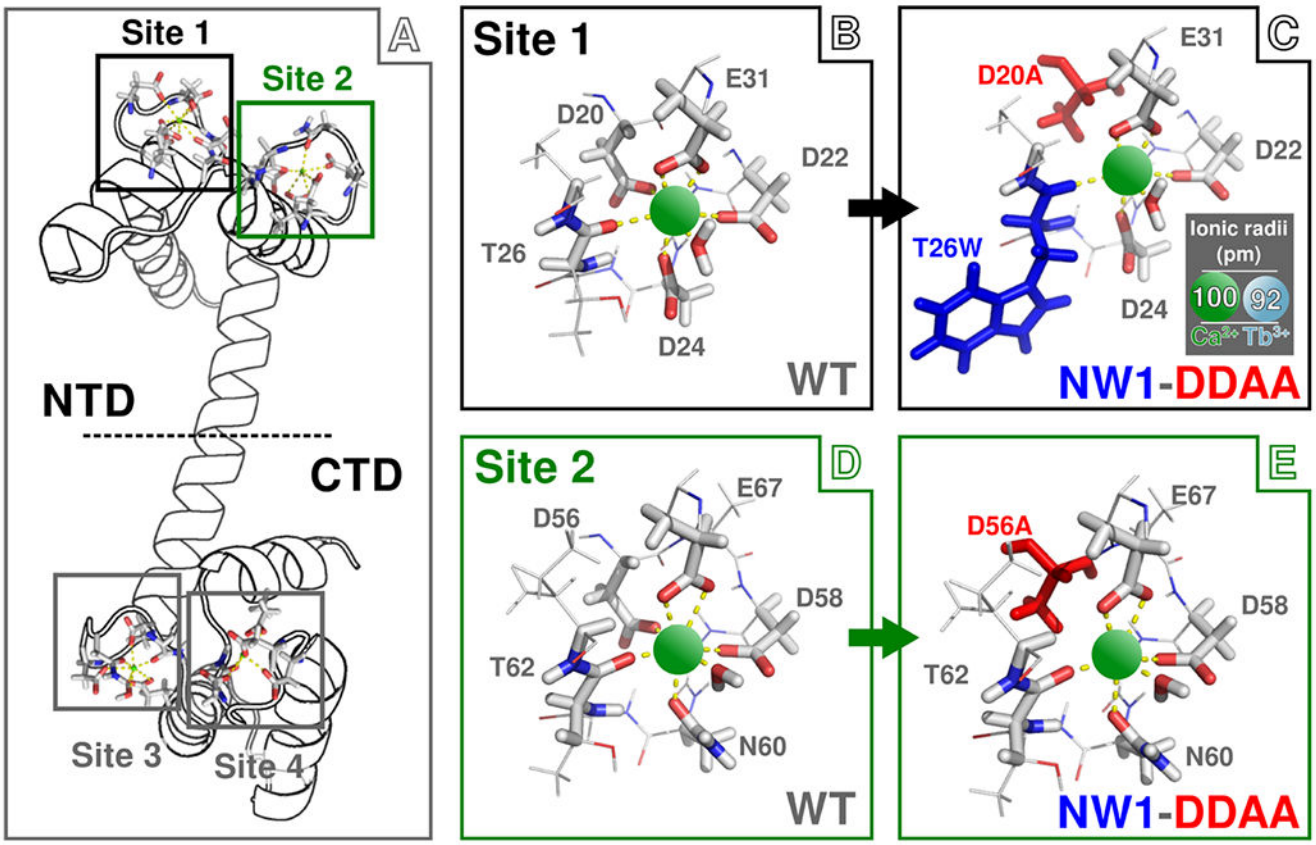

Figure 1.

Schematic representation of the wild-type (WT) and mutant N-CaMs used in this study bound to Ca^{2+}. (A) Structure of full-length WT CaM. Binding site (BS) locations are highlighted by black (BS 1), green (BS 2), and gray (BS 3 and BS 4) boxes. For this work, we use only the sequence of N-terminal domain (NTD) CaM, which contains BS 1 and BS 2 and appears above the dashed horizontal line. (B) Structure of WT BS 1. Ca^{2+} ions are shown as green spheres connected by yellow dashed lines to carboxylate and carbonyl groups responsible for coordination within the binding site. (C) Structure of BS 1 with both NW1 (colored blue) and DDAA (colored red) mutations. (D) Structure of WT BS 2. (E) Structure of BS 2 with both the NW1 and DDAA mutations. Note that the NW1 mutation affects only BS 1; thus, BS 2 of the NW1 mutant is the same as WT. The DDAA mutant involves mutation of both aspartate 20 in BS 1 and aspartate 56 in BS 2 to alanine; thus, the DDAA mutant involves aspartate-to-alanine mutations in both BS but no insertion of tryptophan in either site. The NW1-DDAA mutant combines both the NW1 and DDAA mutations. The inset in panel C shows the relative sizes of the Ca^{2+} and Tb^{3+} to scale with the BS structure. Note that these structures are shown only for illustration of point mutation; actual binding site structures differ and are both sequence-and ion-dependent.

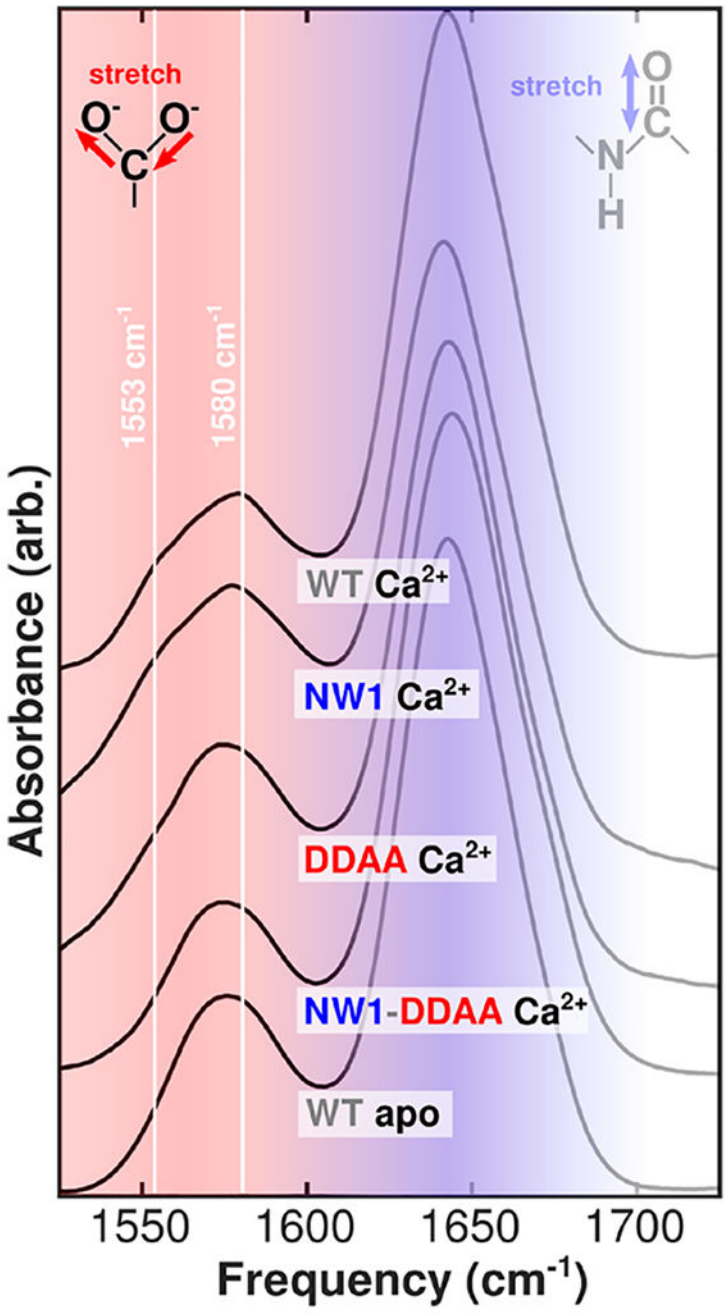

Figure 2.

Selected FTIR spectra of N-CaM bound to Ca^{2+} and Tb^{3+}. Spectra for all structures are included in Figure S1, and corresponding second-derivative spectra are included in Figure S2. Solid white lines highlight peaks corresponding to different modes of carboxylate ion coordination in Ca^{2+}-N-CaM. The bidentate glutamate peak is visible in the Ca^{2+}-bound spectrum at 1553 cm^{-1}, while the monodentate peak is visible at 1580 cm^{-1}. Large, broad absorptions around 1640 cm^{-1} (shaded blue) are amide I modes in the protein backbone, which report on global structure. The carboxylate region centered around 1575 cm^{-1} (shaded

red) reports on local structure in the ion binding sites and is highlighted as the focus of our study.

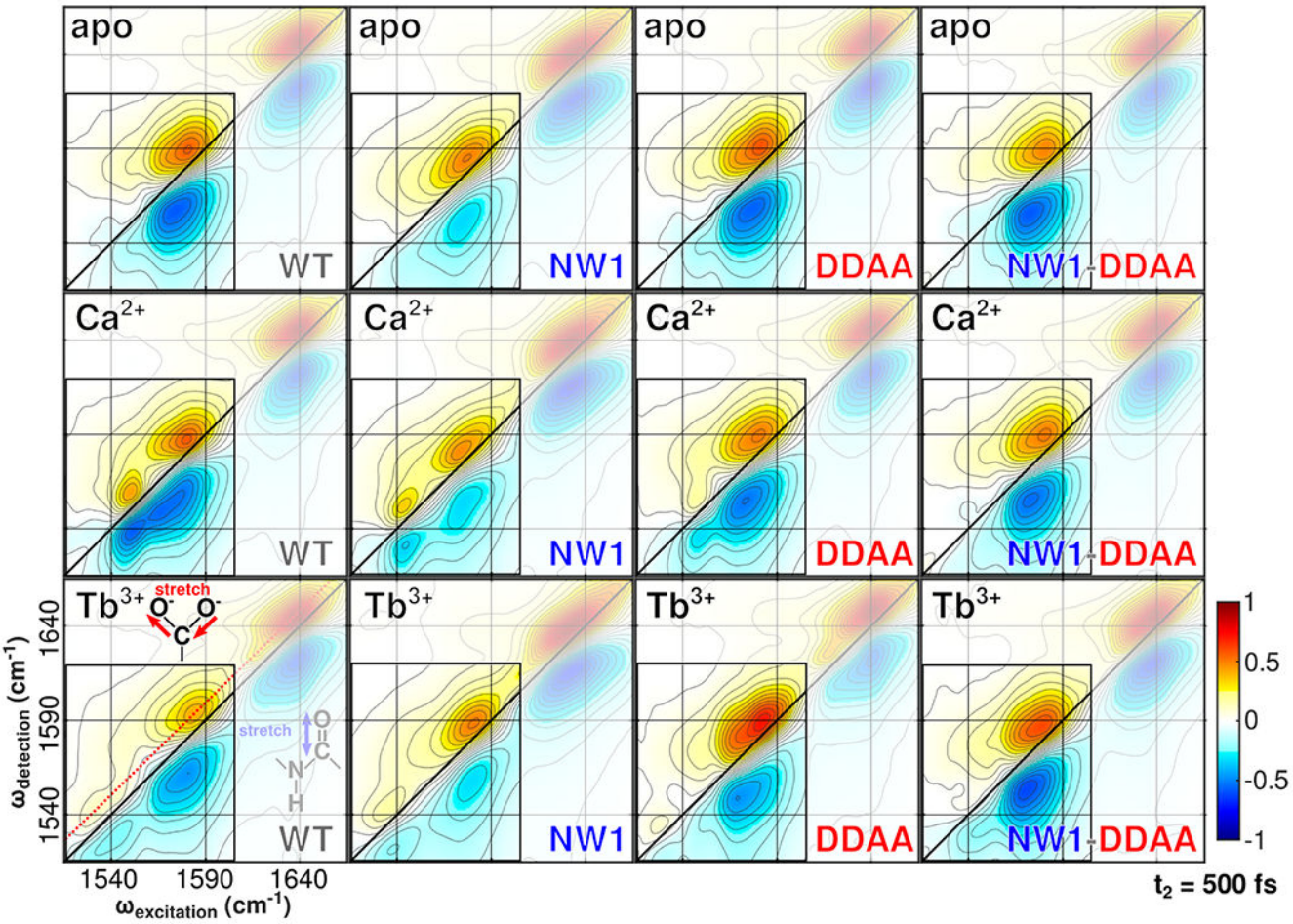

Figure 3.

2D IR spectra of WT and mutant N-CaM bound to Ca^{2+} and Tb^{3+} taken with a pump–probe delay time (t_2) of 500 fs. The dashed red line in the bottom left panel highlights the location of the diagonal slices shown in Figure 4. The bidentate glutamate peak is visible in the Ca^{2+}-bound spectrum near 1553 cm^{-1}, while the monodentate peak is visible near 1580 cm^{-1}. Absorptions around 1640 cm^{-1} are amide I modes in the protein backbone. The carboxylate region centered around 1575 cm^{-1} is highlighted as the focus of our study and reports on local structure in the binding sites. The amide I region contains information about protein secondary structure[42] but is not interpreted in this work. Intensities are normalized to the strongest feature in each spectrum, which is the amide I peak in all cases.

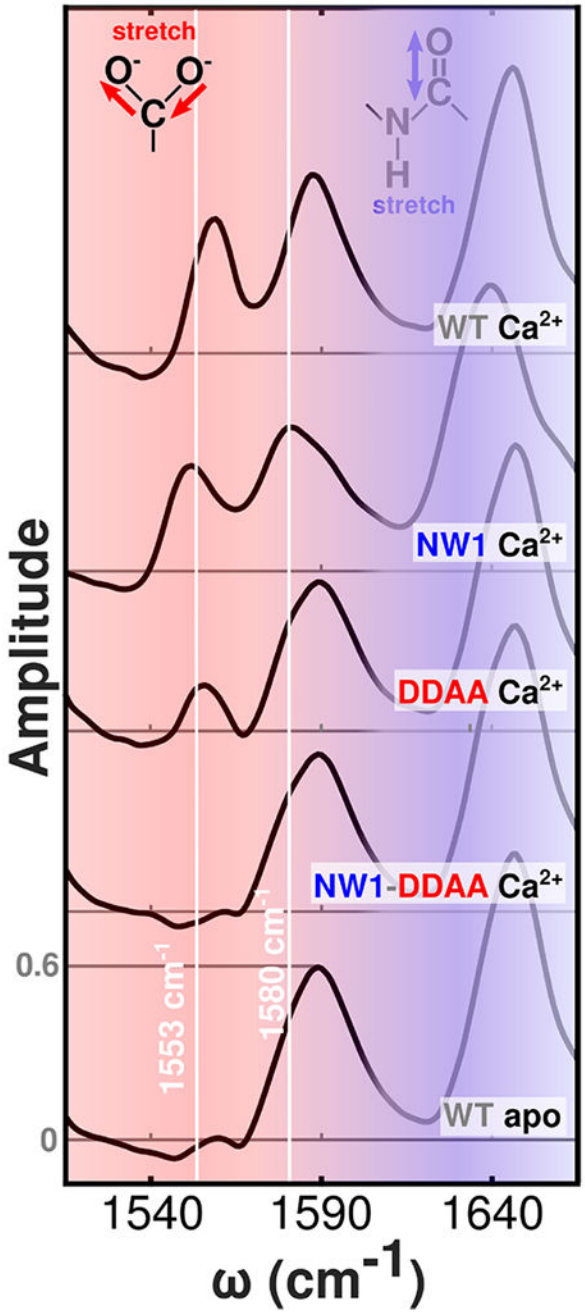

Figure 4.

Selected 2D IR diagonal slices of WT and mutant N-CaM bound to Ca^{2+} and Tb^{3+}. These slices are extracted from the 2D IR data shown in Figure 3. The complete set of slices is included in Figure S3. To facilitate comparison with FTIR spectra, shading, frequency guide lines, and ordering of spectra are the same as in Figure 2. Note that the frequency axis is narrower than in Figure 2 due to the frequency range of the 2D IR measurements.

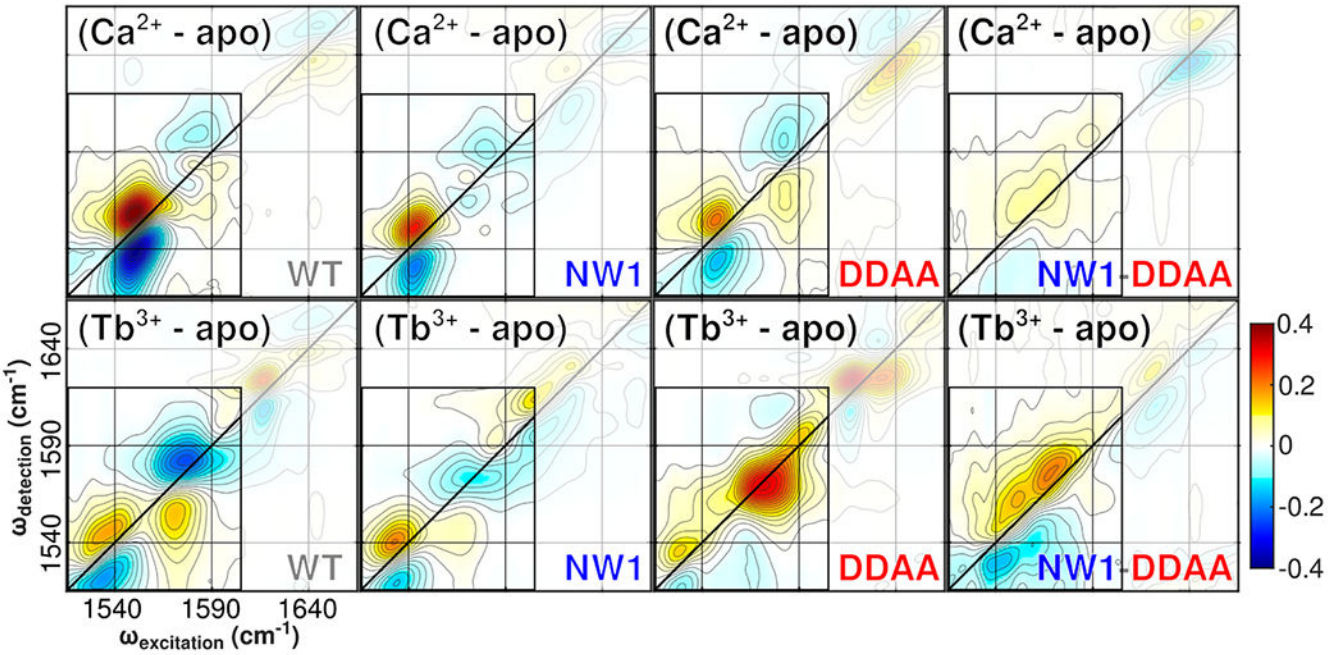

Figure 5.

2D IR difference spectra extracted from the 2D IR data shown in Figure 3. Difference spectra are calculated by subtracting the apo spectrum from the Ca^{2+} and Tb^{3+} spectra for each mutant. The difference spectra thus highlight the specific spectral signatures of Ca^{2+} and Tb^{3+} binding relative to the unbound protein. Note that the color scale covers a narrower range than in Figure 3 to highlight weaker features.

Table 1.

Relative Intensities of Spectral Features from 2D IR Slices in Figure 4[a]

WT Ca^{2+}		NW1 Ca^{2+}		DDAA Ca^{2+}		NW1-DDAA Ca^{2+}		WT apo	
S_{bi}	S_{mono}	S_{bi}	S_{mono}	S_{bi}	S_{mono}	S_{bi}	S_{mono}	S_{bi}	S_{mono}
0.47	0.62	0.37	0.50	0.16	0.52	<0.01	0.55	<0.01	0.60

[a] S_{mono}, amplitude of the monodentate carboxylate peak; S_{bi}, amplitude of the bidentate carboxylate peak. All amplitudes are reported as a fraction of the amide I peak amplitude for each sample.